Simulation strategies and signatures of chaos in classical nonlinear response

Christoph Dellago[1] and Shaul Mukamel[1,2]

[1]*Department of Chemistry, University of Rochester, Rochester, New York 14627*
[2]*Department of Physics and Astronomy, University of Rochester, Rochester, New York 14627*
(Received 2 October 2002; published 31 March 2003)

Algorithms are presented for overcoming the computational challenge of nonlinear response functions which describe the response of a classical system to a sequence of n pulses and depend on nth order multipoint stability matrices containing signatures of chaos. Simulations for the Lorentz gas demonstrate that finite field algorithms can be effectively used for the robust, long time calculation of nonlinear response functions. These offer the possibility to characterize chaos beyond the commonly used Lyapunov exponents and suggest new experimentally accessible measures of chaos.

Response theory offers a convenient framework for connecting the reaction of dynamical systems to an external perturbation with the microscopic dynamics [1]. Van Kampen had raised some insightful objections to this formalism, arguing that in nonlinear dynamical systems the perturbative expansion in the external field may hold only for infinitely short times [2]. Common experience and theoretical analysis show that while these are valid objections for individual trajectories, the problem is cured once a proper ensemble average is carried out [3].

The long debate around this issue was narrowly focused on the linear response. However, the nonlinear response of a dynamical system to a sequence of pulses carries much more detailed information. Nonlinear response functions (NRF) are readily accessible by numerous spectroscopic techniques. Multidimensional NMR [4] and its recent extension to optical and infrared pulses [5] have the capacity to control coherence and probe correlations of dynamical events. In this paper, we show how the NRF may be recast using a hierarchy of stability matrices $M^{(n)}$ which provide new measures of classical chaos. Lyapunov exponents commonly used in the analysis of chaotic systems are related to the lowest member of the hierarchy $M^{(1)}$. We further analyze the merits of equilibrium vs nonequilibrium simulation strategies and specify conditions whereby these higher measures of chaos may be reproduced experimentally.

Consider a system with Hamiltonian $\mathcal{H}(x)$ coupled to a spatially homogeneous field $E(t)$ through $\mathcal{H}'(x,t) = -E(t)A(x)$, where x is a point in phase space and $A(x)$ is an arbitrary phase space variable. To nth order in the applied field the expectation value of an observable B is [6]

$$B^{(n)}(t) = \int_0^t d\tau_n \int_0^{\tau_n} d\tau_{n-1} \cdots \int_0^{\tau_2} d\tau_1 E(\tau_n)$$
$$\times E(\tau_{n-1}) \cdots E(\tau_1) S^{(n)}(t,\tau_n,\tau_{n-1},\ldots,\tau_2,\tau_1). \tag{1}$$

The nth order NRF describing the response at time t to n short pulses at times $\tau_1,\ldots,\tau_n$ is given by

$$S^{(n)}(t,\tau_n,\tau_{n-1},\ldots,\tau_2,\tau_1)$$
$$= \langle\!\langle B | \mathcal{G}(t-\tau_n) \cdots \tilde{A}\mathcal{G}(\tau_2-\tau_1)\tilde{A} | \rho_{\text{eq}} \rangle\!\rangle. \tag{2}$$

Here, $\{A,B\} \equiv \tilde{A}B = \omega_{ij}(\partial A/\partial x_i)(\partial B/\partial x_j)$ is the Poisson bracket for two arbitrary phase space variables $A(x)$ and $B(x)$, Einstein's summation convention is assumed and ω_{ij} takes values $-1, 0,$ and 1. $\langle\!\langle \cdots \rangle\!\rangle$ denotes a matrix element in Liouville space which is calculated as follows: We start with the equilibrium phase space distribution ρ_{eq}. Each of the n actions of the external field on the distribution is represented by a Poisson bracket $\tilde{A}$. In the time intervals between actions the time evolution is described by $\mathcal{G}(\tau) \equiv \exp(-i\mathcal{L}\tau)$, where $\mathcal{L} = \tilde{\mathcal{H}}$ is the Liouville operator. Finally, we multiply the evolved distribution with B and take the trace.

$S^{(n)}$ can be evaluated by acting with all Poisson brackets to the left. Using this *Heisenberg picture* (operators change with time), we find that $S^{(n)}$ can be written in terms of an $(n+1)$time nth order stability matrix,

$$M^{(n)}_{i_{n+1},\ldots,i_1} \equiv \frac{\partial^n x_{i_1}(\tau_1)}{\partial x_{i_{n+1}}(\tau_{n+1}) \cdots \partial x_{i_2}(\tau_2)}. \tag{3}$$

The appearance of stability matrices $M^{(n)}$ provides exciting possibilities for the direct observation of chaos.

Alternatively, we can let the Poisson brackets act to the right. In this *Schrödinger picture* (phase space density changes with time) one can use the identity $\{A,\rho_{\text{eq}}\} = -\beta\dot{A}\rho_{\text{eq}}$ to reduce the highest stability matrix degree by one to $M^{(n-1)}_{i\cdots}$. In particular, the stability matrix cancels out for first order and the linear response contains no signatures of chaos:

$$S^{(1)}(t,\tau_1) = \frac{d}{d\tau_1}\beta\langle B(t)A(\tau_1)\rangle. \tag{4}$$

This *fluctuation dissipation theorem* [1] connects the observable linear response function $S^{(1)}$ with an equilibrium correlation function of the unperturbed system. For higher orders, the stability matrices survive and NRFs carry signatures of chaos [7,8].

Let us first examine the response to a single intense short pulse perturbing the system at $t=0$. The expressions for the corresponding response functions become especially compact if the observables A and B are phase space variables. Let

us assume $A = x_1$ and $B = p$, where p is the momentum conjugate to x_1. In the Heisenberg picture, the single-pulse response function of order n is

$$S^{(n)}(t,0) = \left\langle \frac{\partial^n p(t)}{\partial p^n(0)} \right\rangle = \langle M^{(n)}(t,0) \rangle. \qquad (5)$$

However, the first few response functions in the Schrödinger picture are $S^{(1)}(t) = (\beta/m)\langle p(0)p(t) \rangle$, $S^{(2)}(t) = (\beta/m)^2 \langle p^2(0)p(t) \rangle - (\beta/m)\langle p(t) \rangle$, and $S^{(3)}(t) = (\beta/m)^3 \langle p^3(0)p(t) \rangle - 3(\beta/m)^2 \langle p(0)p(t) \rangle$. Thus, for a single pulse, a fluctuation dissipation like relation holds for response of arbitrary order and the stability matrices can still be eliminated from all higher order response functions.

In contrast, multipulse NRFs explicitly depend on $M^{(n)}$ and cannot be written in terms of correlation functions alone. For example, the second-order response is

$$S^{(2)}(t,\tau_2,\tau_1) = \beta^2 \frac{d^2}{d\tau_1 d\tau_2} \langle B(t)A(\tau_2)A(\tau_1) \rangle$$

$$- \beta \frac{d}{d\tau_1} \langle B(t)\omega_{ij} M_{jk}^{(1)}(\tau_2,\tau_1)A_i'(\tau_2)A_k'(\tau_1) \rangle, \qquad (6)$$

where $A_i' \equiv \partial A / \partial x_i$. Such multipulse (multidimensional) NRFs carry additional most valuable information connected to the ability to observe correlation effects between the dynamics in various time intervals. This is what enables multidimensional NMR to determine the structure of complex molecules [4]. Recent work has extended these ideas to the optical and infrared regimes. In particular, the field of fifth-order Raman spectroscopy of liquids [9] has triggered extensive simulation activity [10–12]. Both equilibrium and finite field techniques were successfully used to calculate higher order NRFs in the short time regime (~ 200 fs). The following simulations examine the merits of these two approaches.

We have performed numerical simulations for the two-dimensional Lorentz gas [13] consisting of a point particle of mass m moving with momentum p through an infinite array of circular scatterers with radius R arranged on a triangular lattice. When the particle collides with a scatterer it is reflected elastically. Between collisions it moves on straight lines with constant velocity. To avoid difficulties in the calculation of stability matrices at collisions, the interaction potential $V(r)$ of the particle with the scatterer is assumed to be steep but smooth instead of impulsive. For $r < R$, $V(r) = \alpha(1 - r^2)^2$ and it vanishes otherwise. In all simulations $\alpha = 10^{10}$. At collisions the equations of motion are integrated with the velocity Verlet algorithm [14]. The scatterer density is $\rho = 4/5\rho_0$, where ρ_0 is the close packed density at which the scatterers are in contact, and canonical initial conditions are assumed. Throughout, length is measured in units of R, energy in units of $k_B T$, mass in units of m, momentum and field strength in units of $(mk_B T)^{1/2}$, velocity in units of $(k_B T/m)^{1/2}$, and time in units of $(mR^2/k_B T)^{1/2}$.

At equilibrium, the average current $j \equiv \langle p_x \rangle / m$ along x vanishes. But after a perturbation $E(t)$ coupling to the posi-
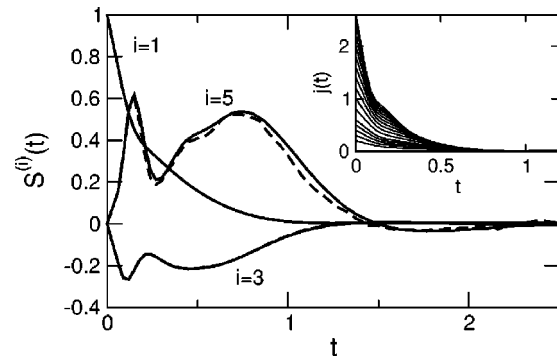
FIG. 1. First-, third-, and fifth-order response functions obtained from equilibrium simulations (solid lines) and nonequilibrium simulations (dashed lines). (For $i=1$ and $i=3$ the equilibrium and nonequilibrium results are indistinguishable on the scale of the figure.) The inset contains the nonequilibrium currents $j(t)$ for various field strengths E.

tion q_x this current $j(t)$ may have a finite value. For small perturbations, the relaxation of $j(t)$ can be predicted from linear response theory, but for larger perturbations, higher order response functions must be taken into account.

Let us first examine the numerical stability of the response to a single impulsive perturbation $E\delta(t)$. Averaging over trajectories started at canonically distributed initial conditions, we determined equilibrium correlation functions $\langle p_x(0)p_x(t) \rangle$, $\langle p_x^2(0)p_x(t) \rangle$, $\langle p_x^3(0)p_x(t) \rangle$, etc., from which the response functions $S^{(n)}(t)$ can be calculated. Due to inversion symmetry, even response functions vanish. The first three nonvanishing response functions $S^{(1)}(t)$, $S^{(5)}(t)$, and $S^{(5)}(t)$ obtained from 500×10^6 trajectories are shown in Fig. 1 as solid lines.

Alternatively, we can calculate NRFs using a nonequilibrium simulation strategy which more closely mimics real experiments [10]. An impulsive perturbation $E\delta(t)$ is applied to a canonical distribution of points in phase space, increasing the momentum in x direction by an amount E. The nonequilibrium current $j(t)$ is then obtained by averaging $p_x(t)$ over trajectories initiated at the perturbed phase points. Currents $j(t)$, each obtained from 500×10^6 trajectories, are displayed in the inset of Fig. 1 for several field strengths ranging from $E = 0.2$ to $E = 2.6$.

From the currents $j(t)$, we determined nonlinear response functions $S^{(n)}(t)$ by fitting $j(t) = ES^{(1)}(t) + E^3 S^{(3)}(t)/3! + E^5 S^{(5)}(t)/5! + E^7 S^{(7)}(t)/7! + E^9 S^{(9)}(t)/9!$ to the numerically determined currents. The resulting response functions are shown in Fig. 1 (dashed lines) along with the equilibrium results (solid lines). The excellent agreement validates the nonequilibrium method. While $S^{(1)}$ shows a simple monotonic decay, $S^{(3)}$ and $S^{(5)}$ display further features originating in multiple correlated collisions.

We next turn to higher order multitime response functions which can be extracted from equilibrium trajectories by using expressions such as Eq. (6), involving higher order stability matrices $M^{(i)}$. In the practical application of these equations, however, numerical difficulties arise due to the exponential growth of stability matrix elements originating in the sensitivity of initial conditions to small perturbations,
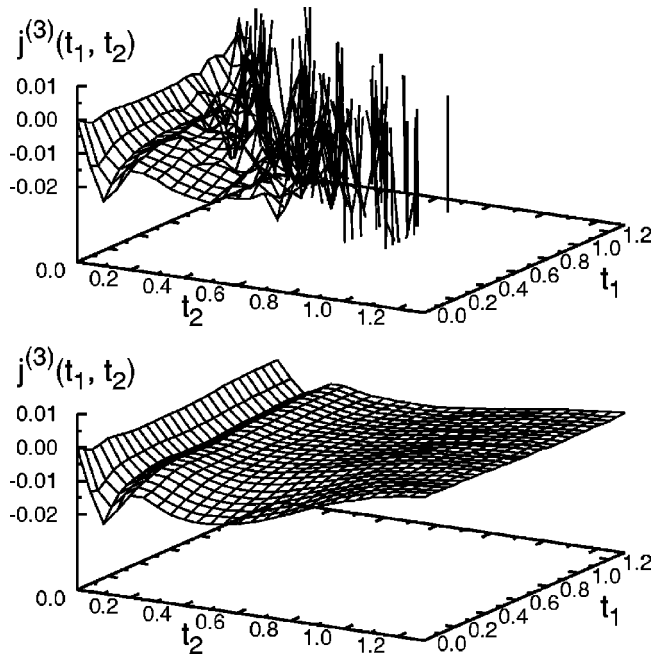
FIG. 2. Third-order response to two short pulses of strength E $=0.4$ as a function of $t_1 \equiv \tau_2 - \tau_1$ and $t_2 \equiv t - \tau_2$ obtained from equilibrium (top) and nonequilibrium simulations (bottom).

FIG. 3. Top: averages $\langle M_{33}^{(i)}(t) \rangle$ for $i = 1$ and 2 as a function of time. Also shown is the time correlation function $\langle p_x(0)p_x(t) \rangle$ (dashed line). Bottom: logarithm of the variance of $M_{33}^{(i)}(t)$ for $i = 1$ and 2.

known as *Lyapunov instability*. As a consequence, the convergence of averages such as those appearing in Eq. (6) is extremely slow and, in practice, they can be accurately evaluated only for very short times.

To illustrate this numerical difficulty we have calculated the third-order response of the Lorentz gas to two short pulses of equal magnitude E acting at times τ_1 and τ_2. In this case, the third-order response $j^{(3)}(t, \tau_2, \tau_1)$ can be written in terms of $S^{(3)}$, which in the Schrödinger representation involves stability matrices up to order two. Although these stability matrices can be readily determined along equilibrium trajectories, our simulations indicate that due to the Lyapunov instability the calculation of $j^{(3)}$ in the Schrödinger representation is impossible but for extremely short times. This difficulty can be mitigated by acting with two $\tilde{A}$ to the right and one to the left. In this intermediate representation (between Schrödinger and Heisenberg) the highest order stability matrix is $M^{(1)}$ instead of $M^{(2)}$. Since the exponential growth is faster for higher order stability matrices, this reduction in order improves the convergence of averages allowing calculation of $j^{(3)}$ to longer times. Results obtained for $E = 0.4$ from 50×10^6 trajectories are shown in Fig. 2 (top). It is, however, evident that even in the intermediate representation the third-order response cannot be reliably calculated if $t_1 + t_2 > 1$.

Using the alternative, finite field approach, we perturbed a set of canonically distributed initial conditions with a short pulse $E_1 \delta(t)$ (here, we set $\tau_1 = 0$). Then, starting from these perturbed initial conditions trajectories were integrated for a time $t_1 \equiv \tau_2 - \tau_1$, after which a second perturbation $E_2 \delta(t - t_1)$ acted on the system. After another interval of length $t_2 \equiv t - \tau_2$, p_x was measured and averaged over all trajecto-

ries yielding the nonequilibrium current $j(t_1, t_2)$. The third-order term $j^{(3)}$ was determined by subtracting the linear response to the two pulses from the total response (assuming higher order responses are negligible). The resulting $j^{(3)}$ is displayed in Fig. 2 (bottom) for $E_1 = E_2 = 0.4$. In contrast to the equilibrium results, the finite field response is not affected by the Lyapunov instability and can be determined for longer times.
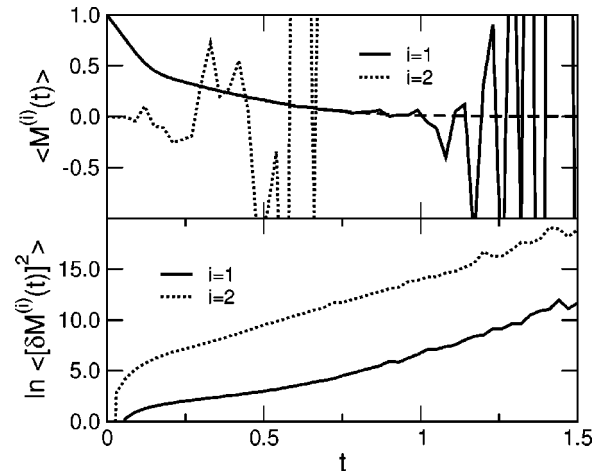
The origin of the numerical problems discussed above can be nicely exemplified by comparing the first-order response function $S^{(1)}$ in the Schrödinger and in the Heisenberg picture. In the former, it is related to the velocity autocorrelation function $S^{(1)}(t) = (\beta/m)\langle p_x(0)p_x(t) \rangle$. This function, computed as an average over 5×10^6 equilibrium trajectories is shown as a dashed line in the top panel of Fig. 3. In the latter, $S^{(1)}(t) = \langle M_{33}^{(1)}(t) \rangle = \langle \partial p_x(t)/\partial p_x(0) \rangle$. Although these expressions are equivalent, the numerical effort required for their calculation differs greatly. In the Schrödinger representation one averages over quantities within the interval $[-1,1]$ and no numerical difficulties arise in this case. The Heisenberg representation, on the other hand, requires averaging over the stability matrix element $\partial p_x(t)/\partial p_x(0)$, a quantity whose magnitude grows exponentially in time and which can be either positive or negative. As a result, the number of trajectories necessary to calculate $S^{(1)}(t)$ with given accuracy grows exponentially with time presenting a practically unsurmountable numerical barrier. This limitation is apparent in the top panel of Fig. 3, in which the solid line denotes the average over the stability matrix. For times $t < 1$ the average stability matrix element coincides with the corresponding velocity autocorrelation function, but then quickly diverges from it, wildly oscillating around the true value. The fast growth of the stability matrix responsible for this behavior is illustrated in the bottom panel. The equality $\langle \partial p_x(t)/\partial p_x(0) \rangle = (\beta/m)\langle p_x(0)p_x(t) \rangle$ (simply obtained by integration by parts) also nicely illustrates how ensemble averaging cures issues such as Van Kampen's criticism of linear response theory. While each stability matrix element ap-

pearing on the left hand side diverges exponentially in time, their average yields an innocuous time correlation function.

The numerical divergence associated with stability matrices becomes stronger as one proceeds to higher order. As an example, the variance of the second-order stability matrix, $\langle [M_{33}^{(2)}(t)]^2 \rangle$, is displayed in the bottom panel of Fig. 3 as a dotted line on a logarithmic scale. The corresponding average $\langle M_{33}^{(2)}(t) \rangle$ is shown in the top panel. Due to symmetry, this average must vanish and any deviation is caused by slow numerical convergence. Thus, the average of the second-order stability matrix can be calculated accurately only for extremely short times. This divergence, absent in finite field simulations, lies at the root of the numerical difficulties in the computation of NRFs with equilibrium methods. Obtaining a numerically stable equilibrium simulation strategy is an open challenge.

Finally, we discuss how these higher signatures of chaos may be probed experimentally. Macroscopic nonlinear response functions are usually well behaved, while individual trajectories have a higher degree of instability and divergence. The extensive phase space averaging eliminates these discrepancies. In order to observe the stability matrices, one should use the ability to control the phase space distribution at various times in the course of the response. Optical pulses can do that. Coherent control algorithms [15] have been devised towards moving wave packets to a desired place or even controlling chemical reactivity. Such methods may be used to design experiments where the wave packets are narrow so that the effects of the averaging may be overcome and the genuine chaotic dynamics be observed, for instance, in trajectories of single molecules subjected to mechanical forces [16].

In summary, the multidimensional nonlinear response of classical systems to a sequence of n short pulses contains valuable dynamical information that can be recast in terms of n point correlation functions and nth order stability matrices $M^{(n)}$. $M^{(1)}$ is commonly used in the study and characterization of chaotic systems (Lyapunov exponents). $M^{(n)}$, which has not been studied in detail, should contain a wealth of additional information. Multiple pulse experiments contain specific signatures of such stability matrices and should provide extremely useful insights into chaotic systems. The first pulse in the sequence may be used to prepare a wave packet (doorway state) corresponding to a narrow region of phase space. Subsequent pulses may then probe the dynamics of the wave packet. Some signatures of chaotic dynamics, which disappear upon ensemble averaging, may then be recovered for this narrowly controlled preparation [5,17]. With recent progress in femtosecond pulse shaping, multiple pulse experiments could be targeted to specifically probe signatures of chaos in higher order stability matrices.

[1] R. Zwanzig, *Nonequilibrium Statistical Mechanics* (Oxford University Press, Oxford, 2001).

[2] N.G. van Kampen, Phys. Norv. **5**, 279 (1971).

[3] R. Kubo, M. Toda, and N. Hashitsume, *Statistical Physics II*, 2nd ed. (Springer, New York, 1991).

[4] R.R. Ernst, G. Bodenhausen, and A. Wokaun, *Principles of Nuclear Magnetic Resonance in One and Two Dimensions* (Clarendon Press, Oxford, 1987).

[5] T. Elsaesser, S. Mukamel, M.M. Murnane, and N.F. Scherer, *Ultrafast Phenomena XII* (Springer-Verlag, Berlin, 2000).

[6] S. Mukamel, V. Khidekel, and V. Chernyak, Phys. Rev. E **53**, R1 (1996).

[7] R.B Williams and R.F. Loring, J. Chem. Phys. **113**, 1932 (2000).

[8] Besides the Schrödinger and Heisenberg pictures, there are intermediate representations in which, part of the time evolution is attributed to the phase space distribution and part to the observables.

[9] Y. Tanimura and S. Mukamel, J. Chem. Phys. **99**, 9496 (1993).

[10] T.I.C. Jansen, J.G. Snijders, and K. Duppen, J. Chem. Phys. **114**, 10 910 (2001).

[11] A. Ma and R.M. Stratt, Phys. Rev. Lett. **85**, 1004 (2000); R.A. Denny and D.R. Reichman, Phys. Rev. E **63**, 065101(R) (2001); J. Cao, J. Wu, and S. Yang, J. Chem. Phys. **116**, 3739 (2002).

[12] S. Saito and I. Ohmine, Phys. Rev. Lett. **88**, 207401 (2002).

[13] J. Machta and R. Zwanzig, Phys. Rev. Lett. **50**, 1959 (1983).

[14] M.P. Allen and D.J. Tildesley, *Computer Simulations of Liquids* (Oxford University Press, Oxford, 1987).

[15] R.J. Levis, G.M. Menkir, and H. Rabitz, Science **292**, 709 (2001).

[16] J. Liphardt, S. Dumont, S.B. Smith, I. Tinoco, and C. Bustamante, Science **296**, 1832 (2002).

[17] *Femtochemistry and Femtobiology: Ultrafast Dynamics in Molecular Science*, edited by A. Douhal (World Scientific, Singapore, 2002).